

Control of the Solid-State Chiral Optical Properties of a Supramolecular Organic Fluorophore Containing 4-(2-Arylethynyl)-Benzoic Acid

Noriaki Nishiguchi,^[a] Takafumi Kinuta,^[a] Yoko Nakano,^[b] Takunori Harada,^[c]
Nobuo Tajima,^[d] Tomohiro Sato,^[a] Michiya Fujiki,^[b] Reiko Kuroda,^[c]
Yoshio Matsubara,^{*,[a]} and Yoshitane Imai^{*,[a]}

Abstract: The solid-state chiral optical properties of a 4-(2-arylethynyl)-benzoic acid/amine supramolecular organic fluorophore can be controlled by changing the arylethynyl group of the achiral 4-(2-arylethynyl)-benzoic acid component molecule rather than the chirality of the amine component molecule.

Keywords: chirality · circular dichroism · circularly polarized luminescence · crystal-engineering · fluorescence

Introduction

The solid-state optical property of organic compounds is a very important property in the development of new functional organic materials. In particular, solid-state organic fluorophores have attracted considerable attention in the field of optoelectronics for applications in organic electroluminescence (EL) devices and optical sensors.^[1] Thus far, many solid-state organic fluorophores have been reported that are composed of a single organic molecule. However, recently, two-component supramolecular organic fluorophores have been attracting attention because their optical properties

can be easily controlled by changing the component molecules.^[2] Furthermore, most of the previously reported supramolecular organic fluorophores do not exhibit chirality, and therefore do not show solid-state chiral optical properties, such as solid-state circular dichroism (CD) and circularly polarized luminescence (CPL).

We recently developed a solid-state π -conjugated chiral supramolecular organic fluorophore that was composed of chiral 1-phenylethylamine (**1**) as the chiral unit and 4-[2-(4-methylphenyl)ethynyl]-benzoic acid (**2**) as the π -conjugated fluorescent unit.^[3] The structural characteristics of this chiral supramolecular organic fluorophore is that it is composed of a 2₁-helical columnar hydrogen-bonded and ionic-bonded network structure formed by the association of the carboxylate oxygen of a carboxylic acid anion with the ammonium hydrogen of a protonated amine. In addition, this fluorophore typically exhibits stronger solid-state CPL on complexation. In general, molecules are more-rigidly constrained in the solid state than in the solution state because of the greater influence of neighboring molecules in the solid state. This influence affords another characteristic of solid-state two-component supramolecular organic fluorophores, with novel functionality resulting from synergy of the two-component molecules. Thus, it is expected that the chiral optical properties of two-component supramolecular organic fluorophores can be controlled by changing the packing structure of the complex. Usually, to control the sign of the chiral optical properties, a chiral compound with opposite chirality is used. However, chiral compounds with opposite chiralities may not be easily available. Therefore, controlling the sign of the chiral optical properties of a chiral fluorophore with-

[a] N. Nishiguchi, T. Kinuta, T. Sato, Prof. Dr. Y. Matsubara, Dr. Y. Imai
Department of Applied Chemistry
Faculty of Science and Engineering, Kinki University
3-4-1 Kowakae, Higashi-Osaka, Osaka 577-8502 (Japan)
Fax: (+81) 6-6727-2024
E-mail: y-imai@apch.kindai.ac.jp
y-matsu@apch.kindai.ac.jp

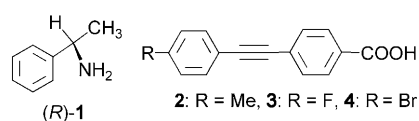
[b] Y. Nakano, Prof. Dr. M. Fujiki
Graduate School of Materials Science
Nara Institute of School and Technology
Takayama, Ikoma, Nara, 630-0192 (Japan)

[c] Dr. T. Harada, Prof. Dr. R. Kuroda
Department of Life Sciences
Graduate School of Arts and Sciences
The University of Tokyo
3-8-1 Komaba, Meguro-ku, Tokyo 153-8902 (Japan)

[d] Dr. N. Tajima
Computational Materials Science Center
National Institute for Materials Science
1-2-1 Sengen, Tsukuba, Ibaraki 305-0047 (Japan)

out using a chiral compound with opposite chirality is instrumental in the development of novel chiral fluorescent systems.

Herein, we report the control of the solid-state chiral optical properties of a chiral two-component supramolecular organic fluorophore—4-(2-arylethynyl)-benzoic acid/amine supramolecular fluorophore—by changing the type of the arylethynyl group in the achiral 4-(2-arylethynyl)-benzoic acid component molecule, and not the chirality of the chiral amine component molecule. (*R*)-(+)-1-phenylethylamine [(*R*)-**1**] was used as the chiral amine component molecule. Two types of 4-(2-arylethynyl)-benzoic acids—4-[2-(4-fluorophenyl)ethynyl]-benzoic acid (**3**) and 4-[2-(4-bromophenyl)ethynyl]-benzoic acid (**4**)—that contain different substituents were used as the achiral 4-(2-arylethynyl)-benzoic acid component molecule in place of **2**.



Results and Discussion

The (*R*)-**1/3** [or (*R*)-**1/4**] chiral supramolecular organic fluorophore was prepared by crystallization from an ethanol (EtOH) solution in the same manner as that used for the preparation of (*R*)-**1/2** supramolecular organic fluorophore **I**. (*R*)-**1** and **3** (or **4**) were dissolved in ethanol and left to stand at room temperature. After a week, a large number of crystals of **II**, composed of (*R*)-**1** and **3** (or crystals of **III** composed of (*R*)-**1** and **4**) were obtained.

The most-serious complication associated with solid-state organic fluorophores is the occurrence of fluorescence quenching in the crystalline state. In order to study the solid-state optical properties of obtained complexes **II** and **III**, their solid-state fluorescence spectra were first measured. Both complexes exhibited fluorescence. The solid-state fluorescence maximum (λ_{em}) of complex **II** was observed at 423 nm, and the absolute value of the photoluminescence quantum yield (Φ_F) was 0.32 in the solid state. On the other hand, the solid-state λ_{em} and Φ_F of complex **III** were 416 nm and 0.21, respectively. In both the complexes, the solid-state λ_{em} value shifted to a longer wavelength relative to that of complex **I** (λ_{em} = 379 nm). It is well known that a small HOMO–LUMO gap induces a red shift of the

emission wavelength.^[4] Hence, the HOMO–LUMO gaps of **2**, **3**, and **4** in the isolated state were studied theoretically. The theoretically calculated HOMO–LUMO gaps of the gas-phase molecules of **2**, **3**, and **4** were 3.98, 4.04, and 3.98 eV, respectively; these HOMO–LUMO gaps have a similar value.

However, the values of the solid-state λ_{em} of the complexes differ according to the type of 4-(2-arylethynyl)-benzoic acid. The solid-state λ_{em} decreases in the order: **II** (λ_{em} = 423 nm) > **III** (λ_{em} = 416 nm) > **I** (λ_{em} = 379 nm). This trend indicates that in this fluorescent system, the difference in solid-state λ_{em} , which depends on the type of arylethynyl group, may have been mainly caused by the difference in the crystal packing of these complexes.

In order to study the trends in the solid-state chiral optical properties (CD and CPL properties) of 4-(2-arylethynyl)-benzoic acid/amine supramolecular fluorophore, the solid-state CD spectra of fluorescent complexes **II** and **III** were measured using KBr pellets; these were also used for similar measurements in the case of complex **I**. The solid-state CD and absorption spectra of complexes **I**,^[3] **II**, and **III** (black lines) are shown in Figure 1.

The shapes of the CD spectra are similar. Characteristic peaks of the ethynylphenylene unit are observed between 294 and 323 nm. The circular anisotropy factors, $|g_{CD} = \Delta OD/OD|$, of the last Cotton effect (λ^{CD} = 320 nm for **I**, 313 nm for **II**, and 323 nm for **III**) for **I**, **II**, and **III** are approximately 1.0×10^{-3} , 4.1×10^{-3} , and 1.5×10^{-3} , respectively. In order to check whether complexes **I–III** introduced any artifacts into the spectrum, complexes **I'–III'** were prepared in which (*R*)-**1** was replaced with (*S*)-(–)-1-phenylethylamine, (*S*)-**1**. The solid-state CD spectra of complexes **I'**,^[3] **II'**, and **III'** were then measured (Figure 1, gray lines). These CD spectra were found to be mirror images of the CD spectra of complexes **I–III**, which indicates that effective chiral transfer occurs from chiral **1** to complexes **II** and **III** through complexation, as in the case of complex **I**.

Interestingly, the signs of the CD spectra of chiral complexes **I–III** (or **I'–III'**) were different to one another, even though they are composed of amine component molecules with the same chirality. That is, the signs of the CD spectra of complexes **I** and **III** at the longest wavelength are positive (+; Figure 1 a and c, black lines) whereas that of complex **II** is negative (–; Figure 1 b, black lines). This observation shows that the solid-state CD property of 4-(2-arylethynyl)-benzoic acid/amine supramolecular organic fluorophore can be controlled by changing the arylethynyl unit in the achiral 4-(2-arylethynyl)-benzoic acid component molecule.

To study the origin of the solid-state CD property of these complexes, X-ray crystallographic analyses of complexes **II** and **III** were carried out, and the crystal structures of complexes **I**,^[3] **II**, and **III** were compared. The crystal structure of **I** is shown in Figure 2. The stoichiometry of **I** is (*R*)-**1/2** = 1:1, and its space group is *P2*₁. This complex has a characteristic 2₁-helical columnar network structure along the *b* axis (Figure 2 a and 2 b). This column is mainly composed of the carboxylate oxygen atoms from the carboxylic

Abstract in Japanese:

本研究では、4-(2-arylethynyl)-benzoic acid/amine 系超分子有機発光体の固体状態におけるキラルな光学特性(円偏光二色性及び円偏光ルミネッセンス)をアミン構成分子のキラリティーではなく、アキラルな 4-(2-arylethynyl)-benzoic acid 構成分子のアリールエチニル基の種類を変えることにより、制御することに成功した。

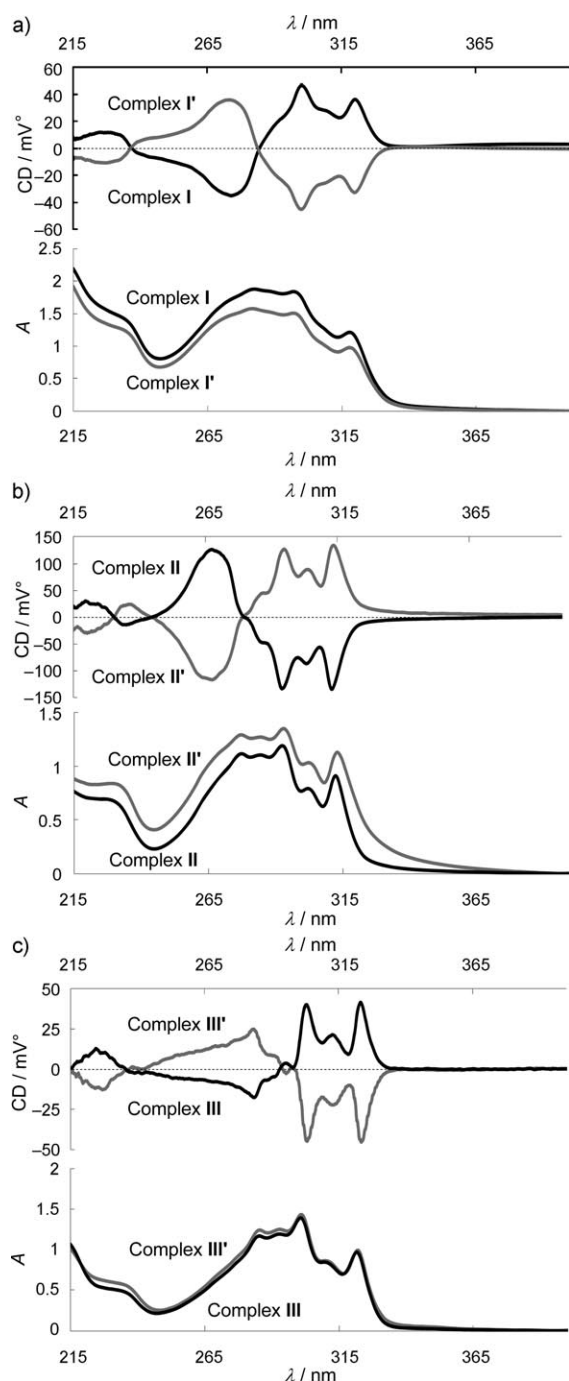


Figure 1. CD and absorption spectra of complexes a) **I**, b) **II**, and c) **III** (black lines) and complexes **I'**–**III'** (gray lines) in the solid state (KBr pellets).

acid anions and the ammonium hydrogen atoms from the protonated amines. Moreover, the intracolumnar benzene–benzene edge-to-face interactions (2.96 Å, Figure 2a, solid arrows *A*) between the hydrogen atom of the benzene ring in **2** and the benzene ring of (*R*)-**1** are also observed.^[5] **I** is formed by the self assembly of these 2_1 -helical columns by three intercolumnar benzene–benzene edge-to-face interactions (2.93, 2.73, and 2.75 Å; indicated by Figure 2c, solid arrows *B*–*D*, and Figure 2d).^[5]

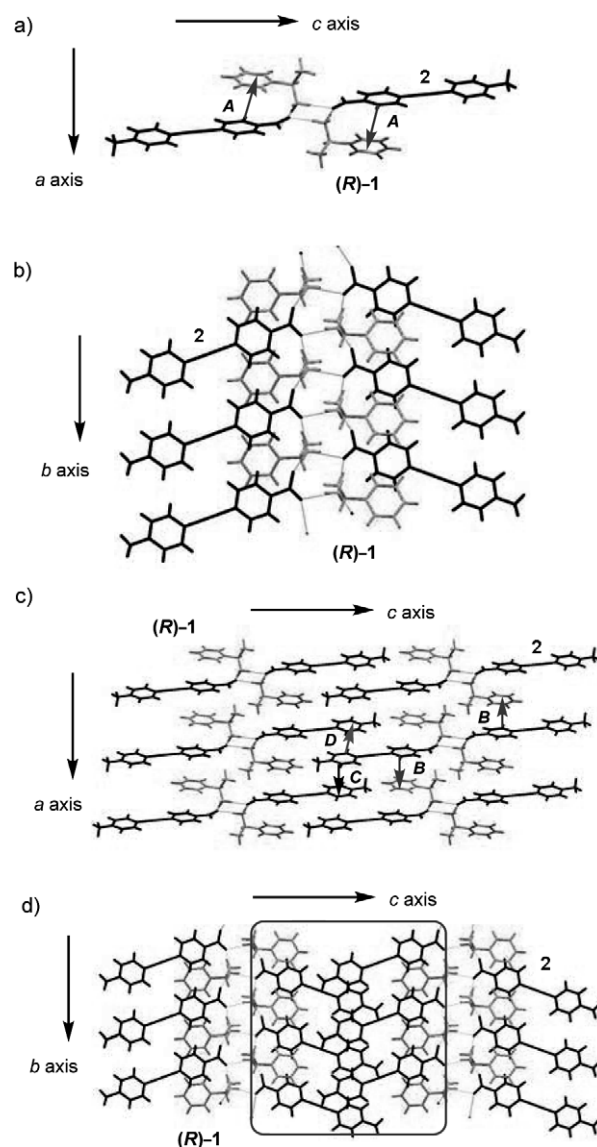


Figure 2. Crystal structure of **I**. a) 2_1 -helical columnar network structure observed along the *b* axis. Solid arrows *A* indicate the intracolumnar benzene–benzene edge-to-face interactions. b) View along the *a* axis. c) Packing structure along the *b* axis. Solid arrows *B*–*D* indicate the intercolumnar benzene–benzene edge-to-face interactions. d) View along the *a* axis.

The crystal structure of **II** is shown in Figure 3. The stoichiometry of **II** is (*R*)-**1**/**3** = 1:1, and its space group is $P2_12_12_1$. This complex also has a 2_1 -helical columnar network structure along the *a* axis, as in complex **I** (Figure 3a and 3b). In complex **II**, intracolumnar benzene–benzene edge-to-face interactions (2.94 Å, indicated by solid arrows *A* in Figure 3a) between the hydrogen atom of the benzene ring in **3** and the benzene ring of (*R*)-**1** were also observed.^[5] **II** was formed by the self-assembly of these 2_1 -helical columns through three intercolumnar benzene–benzene edge-to-face interactions (2.81, 2.76, and 2.79 Å, Figure 3a, solid arrows *B*–*D*, respectively, and Figure 3b).^[5] In addition, two intercolumnar F...H interactions (2.60 Å; indicated by solid arrows *E* and *F*, in Figure 3a) were also observed.^[5] Interest-

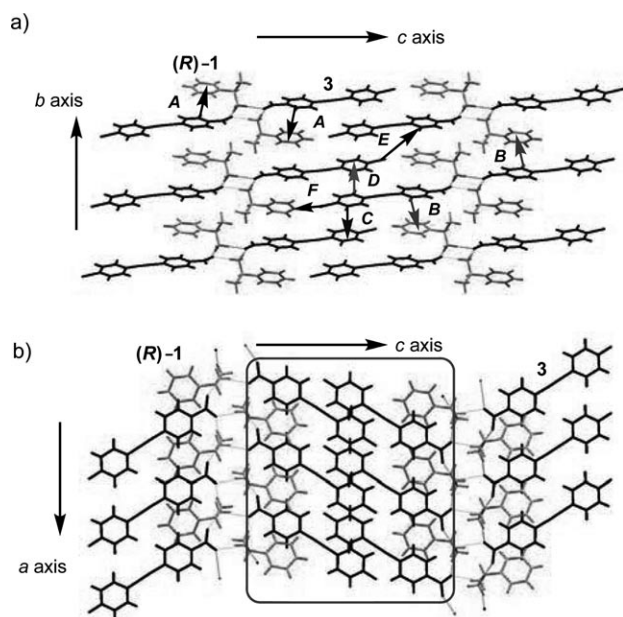


Figure 3. Crystal structure of **II**. a) Packing structure of 2_1 -helical columnar network structure observed along the a axis. Solid arrows A indicate the intracolumnar benzene-benzene edge-to-face interactions. Solid arrows B - D indicate the intercolumnar benzene-benzene edge-to-face interactions. Solid arrows E and F indicate intercolumnar $F\cdots H$ interactions. (b) View along the b axis.

ingly, X-ray crystallographic analyses revealed that although the structures of the 2_1 -helical columns in complexes **I** and **II** are the same, the packing structures of the shared 2_1 -helical columns are considerably different (indicated by solid rectangles in Figure 2d and 3b).

The crystal structure of **III** is shown in Figure 4. The stoichiometry of **III** is $(R)-1/4 = 1:1$, and its space group is $P2_1$, which is the same as that of complex **I**. The shared 2_1 -helical columnar network structure, formed by intracolumnar benzene-benzene edge-to-face interactions (2.93 \AA , Figure 4a, solid arrows A), was observed in this complex (Figure 4a and 4b).^[5] As expected, the packing structures of the shared 2_1 -helical columns in complexes **I** and **III** were identical (rectangles in Figure 2d and 4b); on the other hand, those in complexes **II** and **III** were different (rectangles in Figure 3b and 4b). In **III**, there are three intercolumnar benzene-benzene edge-to-face interactions between the 2_1 -helical columns (2.97 , 2.73 , and 2.71 \AA , Figure 4a, solid arrows B - D , respectively, and Figure 4b).^[5] In addition, one intercolumnar $\text{Br}\cdots\text{H}$ interaction (3.00 \AA ; Figure 4a, solid arrow E) were also observed.^[5]

Complexes **I** and **II** have a set of positive and negative CD intensities in 250 - 330 nm , which originate from the electronic absorption in this region of molecules **2** and **3**, respectively. CD intensities of this type are likely to arise from the coupling of monomer electronic transitions between the neighboring molecules in crystals. The CD intensity of complex **I** in this wavelength region is $+/-$ from the longer-wavelength side whereas that of complex **II** has the opposite sign; i.e., $-/+$ from the longer-wavelength side. To investi-

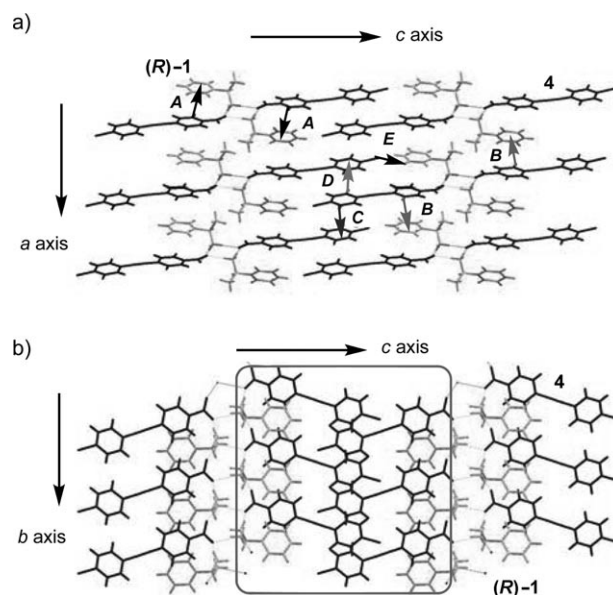


Figure 4. Crystal structure of **III**. a) Packing structure of 2_1 -helical columnar network structure observed along the b axis. Solid arrows A indicate the intracolumnar benzene-benzene edge-to-face interactions. Solid arrows B - D indicate the intercolumnar benzene-benzene edge-to-face interactions. Solid arrow E indicates the intercolumnar $\text{Br}\cdots\text{H}$ interaction. b) View along the a axis.

gate the origin of the observed CD intensities, the excited states of the molecular pairs of **2** and **3** in crystals **I** and **II**, respectively, were calculated theoretically. For this purpose, the nearest molecular pairs were selected, as shown in Figure 5, and their excitation energies and rotational strengths were calculated by Zerner's intermediate neglect of differential overlap (ZINDO) method using the Gaussian 03 program.^[10] Table 1 lists the calculated properties of the

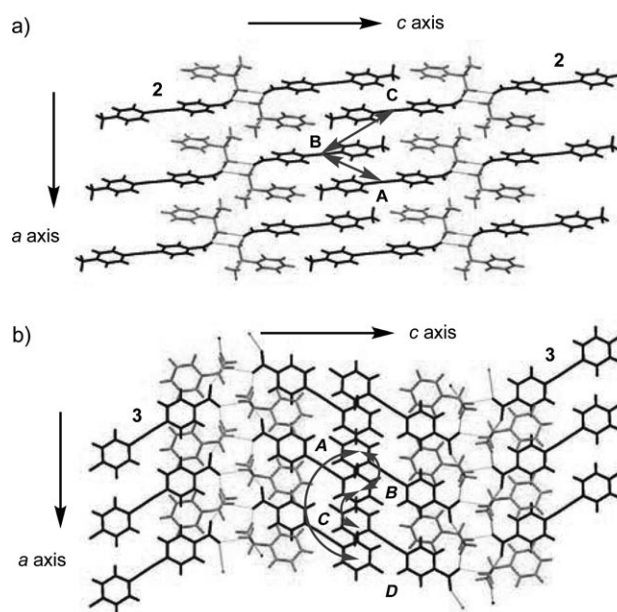


Figure 5. Molecular pairs in a) complex **I** and b) complex **II** whose excited states were calculated theoretically (indicated by arrows).

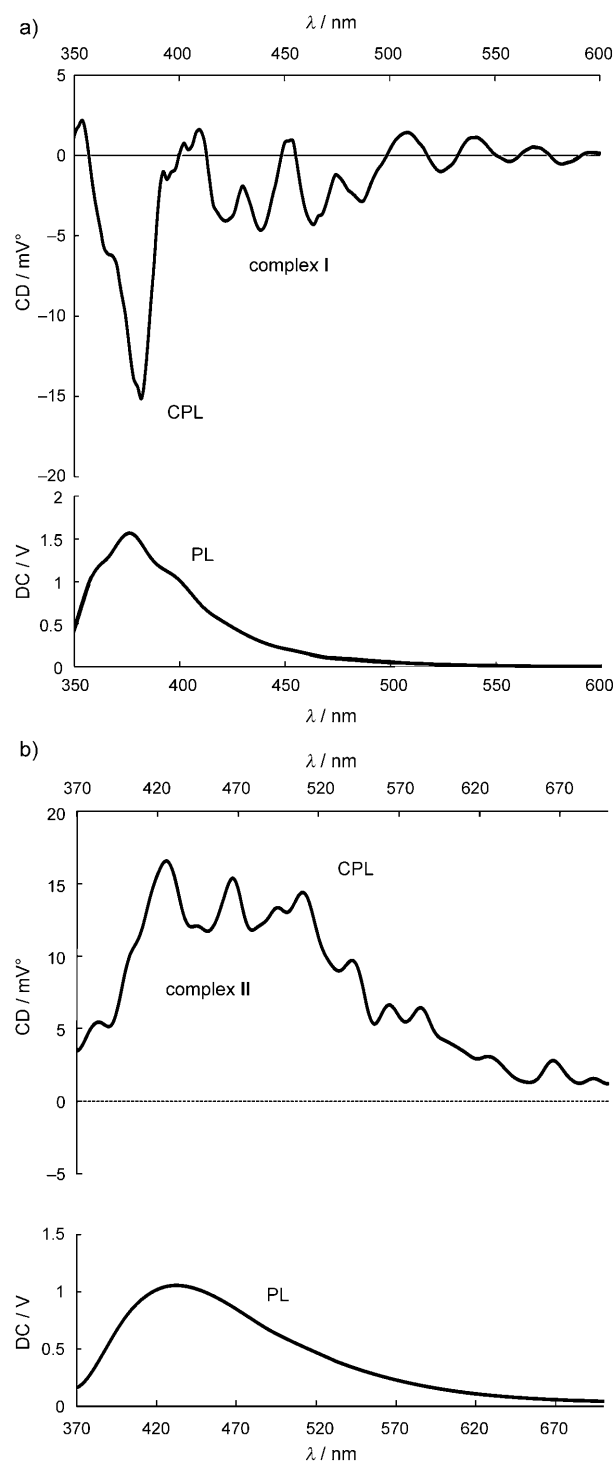
Table 1. Calculated excited states of monomer molecules of **2** and **3** and their molecular dimers in complexes **I** and **II**, respectively.^[a]

	<i>E</i> [eV]	λ [nm]	<i>f</i>	<i>R</i> x10 ⁻⁴⁰ [erg esu cm Gauss ⁻¹]
Complex I				
Monomer ^[b]	3.71	333.8	0.3207	71.3
Dimer A–B ^[c]	3.77	328.9	0.2077	86.2
	3.79	327.2	0.3885	51.0
Dimer B–C ^[c]	3.75	330.7	0.4165	237.4
	3.79	327.3	0.1961	–61.5
Complex II				
Monomer ^[b]	3.67	337.9	0.2939	34.6
Dimer A–B ^[c]	3.73	332.3	0.0196	–47.9
	3.76	329.9	0.5585	128.6
Dimer B–C ^[c]	3.72	333.7	0.6020	23.6
	3.75	330.3	0.0721	66.4
Dimer A–D ^[c]	3.71	333.8	0.0212	–187.2
	3.75	330.4	0.5152	216.4

[a] *E* = excitation energy, λ = excitation wavelength, *f* = oscillator strength (dimensionless), *R* = rotational strength. [b] The strongest electronic transition of monomer molecules, which correspond to the electronic absorption bands of complexes **I** and **II**, occur in the 250–330 nm region. The molecular geometries of the respective crystals were used in the calculations. [c] Excited states of molecular dimers that arise from the coupling of monomer electronic transitions. See Figure 5 for the molecular arrangement of the calculated dimers.

excited states of the dimers; these properties arise from the coupling of the strongest monomer electronic transitions. The calculated results suggest that the sign of the CD intensity of complex **I** (+/– from the longer wavelength side) results from molecular pair B–C rather than molecular pair A–B, and the sign of the CD intensity of complex **II** (–/+ from the longer wavelength side) results from molecular pairs A–B and A–D rather than B–C. It should also be noted that the electronic transition of the monomer molecule in each crystal has significant rotational strength because of the twisted molecular conformation around the C–COO bonds. Thus, the experimentally observed CD intensities are caused by this monomer distortion as well as by the coupling of monomer electronic transitions.

Next, the solid-state CPL spectrum of complex **II** was measured using KBr pellets and compared to that of complex **I**. The solid-state CPL and fluorescence spectra of complexes **I**^[3] and **II** are shown in Figure 6. The fluorescence spectrum of complex **II**, measured using KBr pellets is similar to that of complex **II** obtained without using KBr matrices. This result shows that the KBr matrix does not play any role in the measurement of spectra. A positive CPL spectrum was obtained for complex **II**. The circular anisotropy factor, $g_{em} = 2(I_L - I_R)/(I_L + I_R)$, of complex **II** is approximately $+4.8 \times 10^{-4}$. As expected, a comparison of the CPL property of chiral complex **I** with that of chiral complex **II** indicated that the sign of the CPL spectra changes from negative (–) for **I** to positive (+) for **II**. To the best of our knowledge, this is the first time that the sign of solid-state CD and CPL in a chiral supramolecular organic fluorophore has been controlled by changing the type of the arylethynyl unit in the achiral 4-(2-arylethynyl)-benzoic acid component molecule.

Figure 6. Solid-state CPL and fluorescence spectra of complexes a) **I** and b) **II** (KBr pellets).

Conclusions

A chiral supramolecular organic fluorophore was successfully synthesized by using achiral fluorescent 4-[2-(4-fluorophenyl)ethynyl]-benzoic acid, or 4-[2-(4-bromophenyl)ethynyl]-benzoic acid, and chiral (*R*)-(+)-1-phenylethylamine. By

changing the arylolethynyl unit in achiral 4-(2-arylolethynyl)-benzoic acid from 4-methylbenzene to 4-fluorobenzene, the packing structure of the arylolethynyl unit changed from a planar structure for **I** to an intersection structure for **II**. As a result, the signs of the solid-state CD and CPL spectra of these supramolecular fluorophores were reversed despite using the same chiral-amine component molecule. These results indicate that the solid-state chiral optical properties of 4-(2-arylolethynyl)-benzoic acid/amine supramolecular organic fluorophore can be controlled by changing the type of the arylolethynyl unit in the achiral 4-(2-arylolethynyl)-benzoic acid component molecule (that is, by changing the packing structure of the arylolethynyl unit) instead of changing the chirality of the chiral amine component molecule in the solid state. Supramolecular organic fluorophores offering these functionalities are expected to be useful in the development of novel solid-state chiral supramolecular fluorophores.

Experimental Section

General Methods

Component molecule (*R*)-**1** was purchased from Tokyo Kasei Kogyo Co. Crystallization solvent was purchased from Wako Pure Chemical Industry. This solvent was used directly as obtained commercially.

Synthesis of Compounds **3** and **4**

Component molecules **3** and **4** were prepared by a typical Sonogashira electronic cross-coupling reaction.^[6] Component molecule **3**: ¹H NMR (300 MHz, CD₃COCD₃): δ = 8.07 (d, *J* = 8.1 Hz, 2H), 7.68 (d, *J* = 8.1 Hz, 2H), 7.66 (d, *J* = 8.7 Hz, 2H), 7.24 ppm (d, *J* = 8.7 Hz, 2H). HRMS (EI): *m/z* [M]⁺ Calcd for C₁₅H₉FO₂: 240.0587; found: 240.0651. Component molecule **4**: ¹H NMR (300 MHz, CD₃COCD₃): δ = 8.08 (d, *J* = 8.4 Hz, 2H), 7.69 (d, *J* = 10.2 Hz, 2H), 7.65 (d, *J* = 8.4 Hz, 2H), 7.55 ppm (d, *J* = 10.2 Hz, 2H). HRMS (EI): *m/z* [M]⁺ Calcd for C₁₅H₉BrO₂: 299.9786; found: 299.9932.

Formation of a Complex by Crystallization from Ethanol

(*R*)-**1** (11 mg, 0.10 mmol) and **3** (19 mg, 0.08 mmol) or **4** (24 mg, 0.08 mmol) were dissolved in EtOH (3 mL) and left to stand at room temperature. After a week, a large number of crystals of **II** (14 mg) were obtained, composed of (*R*)-**1** and **3** (or **III** (16 mg), composed of (*R*)-**1** and **4**). The weight reported is the total yield of the crystals obtained in a single batch.

Theoretical Calculations

The HOMO–LUMO band gaps were calculated using hybrid density functional theory (B3LYP functional^[7]) with the cc-pVDZ basis set.^[8] The excitation energies and rotational strengths of molecules and molecular pairs were calculated by the Zerner's intermediate neglect of differential overlap (ZINDO) method.^[9] These quantum chemical calculations were carried out using the Gaussian 03 program.^[10]

Measurement of Solid-State Fluorescence Spectra

Solid-state fluorescence and the absolute photo-luminescence quantum yield were measured by *Absolute PL Quantum Yield Measurement System* (C9920-02, HAMAMATSU PHOTONICS K. K.) under an air atmosphere at room temperature. The excited wavelength is 332, 355, and 365 nm for complexes **I**, **II**, and **III**, respectively.

Measurement of Solid-State CD and Absorption Spectra

The CD and absorption spectra were measured using a *Jasco J-800KCM spectrophotometer*. The solid-state samples were prepared according to the standard procedure for obtaining glassy KBr matrices.^[11]

X-ray Crystallographic Study of Crystal **II**

X-ray diffraction data for single crystals were collected using a *BRUKER APEX*. The crystal structures were solved by the direct method^[12] and refined by full-matrix least-squares using *SHELXL97*.^[12] The diagrams were prepared using *PLATON*.^[13] Absorption corrections were performed using *SADABS*.^[14] Nonhydrogen atoms were refined with anisotropic displacement parameters, and hydrogen atoms were included in the models in their calculated positions in the riding model approximation. Crystallographic data for **II**: C₂₃H₂₀F₁N₁O₂, *M* = 361.40, space group *P*2₁2₁1, *a* = 6.0758(3), *b* = 7.1227(4), *c* = 42.735(2) Å, *V* = 1849.39(17) Å³, ρ_{calc} = 1.298 g cm⁻³, *z* = 4, μ(MoKα) = 0.089 mm⁻¹, 11 408 reflections measured, 4198 unique, final *R*(*F*²) = 0.0377 using 4020 reflections with *I* > 2.0 σ(*I*), *R*(all data) = 0.0397, *T* = 115(2) K. CCDC 769653 (**II**) and 769654 (**III**) contains the supplementary crystallographic data for this paper. These data can be obtained free of charge from The Cambridge Crystallographic Data Centre via www.ccdc.cam.ac.uk/data_request/cif.

X-ray Crystallographic Study of Crystal **III**

Crystallographic data for **III**: C₂₃H₂₀Br₁N₁O₂, *M* = 386.28, space group *P*2₁, *a* = 7.1753(5), *b* = 5.9312(4), *c* = 23.1522(15) Å, β = 97.5860(10)°, *V* = 976.69(11) Å³, ρ_{calc} = 1.313 g cm⁻³, *z* = 2, μ(MoKα) = 2.115 mm⁻¹, 8501 reflections measured, 4249 unique, final *R*(*F*²) = 0.0298 using 3972 reflections with *I* > 2.0 σ(*I*), *R*(all data) = 0.0320, *T* = 115(2) K.

Measurement of the Solid-State CPL Spectrum

The CPL spectrum was measured using a *Jasco CPL-200 spectrophotometer*. The excited wavelength is 350 nm. The solid-state samples were prepared according to the standard procedure for obtaining glassy KBr matrices. The power of an incident beam of the CPL spectrometer is 8.0 μW/0.04 cm² at the installation position of sample. The CPL spectrum is approached by Simple Moving Average (SMA).

Acknowledgements

This study was supported by a Grant-in-Aid for Scientific Research (No. 22750133) from the Ministry of Education, Culture, Sports, Science and Technology, Japan, and MST.

- [1] a) J. Shinar, *Organic Light-Emitting Devices*, Springer, New York, **2004**; b) K. Müllen, U. Scherf, *Organic Light-Emitting Devices*, Wiley-VCH, Weinheim, **2006**; c) C. Jeanne, R. Regis, *Dalton Trans.* **2008**, 6865–6876; d) S. Kappaun, C. Slugovc, J. M. Emil, *Int. J. Mol. Sci.* **2008**, 9, 1527–1547; e) K. Milan, O. Franc, *Acc. Chem. Res.* **2009**, 42, 235–248; f) W.-Y. Wong, C.-L. Ho, *J. Mater. Chem.* **2009**, 19, 4457–4482; g) K.-L. Chan, P. Sonar, A. Sellinger, *J. Mater. Chem.* **2009**, 19, 9103–9120; h) F. Laquai, Y.-S. Park, J.-J. Kim, T. Basche, *Macromol. Rapid Commun.* **2009**, 30, 1203–1231; i) C. Wang, J. Zhang, K. Ryu, A. Badmaev, L. G. D. Arco, C. Zhou, *Nano. Lett.* **2009**, 9, 4285–4291; j) M.-K. Wei, C.-W. Lin, C.-C. Yang, Y.-W. Kiang, J.-H. Lee, H.-Y. Lin, *Int. J. Mol. Sci.* **2010**, 11, 1527–1545 and the references therein.
- [2] a) Y. Mizobe, N. Tohnai, M. Miyata, Y. Hasegawa, *Chem. Commun.* **2005**, 1839–1841; b) Y. Mizobe, H. Ito, I. Hisaki, M. Miyata, Y. Hasegawa, N. Tohnai, *Chem. Commun.* **2006**, 2126–2128; c) S. Oshita, A. Matsumoto, *Langmuir* **2006**, 22, 1943–1945; d) Y. Mizobe, M. Miyata, I. Hisaki, Y. Hasegawa, N. Tohnai, *Org. Lett.* **2006**, 8, 4295–4298; e) Y. Imai, K. Kawaguchi, T. Harada, T. Sato, M. Ishikawa, M. Fujiki, R. Kuroda, Y. Matsubara, *Tetrahedron Lett.* **2007**, 48, 2927–2930; f) Y. Imai, K. Murata, K. Kawaguchi, T. Sato, R. Kuroda, Y.

- Matsubara, *Org Lett.* **2007**, *9*, 3457–3460; g) Y. Mizobe, T. Hinoue, M. Miyata, I. Hisaki, Y. Hasegawa, N. Tohnai, *Bull. Chem. Soc. Jpn.* **2007**, *80*, 1162–1172; h) Y. Imai, K. Murata, K. Kawaguchi, T. Sato, N. Tajima, R. Kuroda, Y. Matsubara, *Chem. Asian J.* **2008**, *3*, 625–629; i) Y. Imai, K. Nagasaki, K. Murata, K. Kawaguchi, T. Harada, Y. Nakano, T. Sato, M. Fujiki, R. Kuroda, Y. Matsubara, *CrystEngComm* **2008**, *10*, 951–953; j) Y. Imai, K. Kamon, K. Murata, T. Harada, Y. Nakano, T. Sato, M. Fujiki, R. Kuroda, Y. Matsubara, *Org. Biomol. Chem.* **2008**, *6*, 3471–3475; k) Y. Ooyama, K. Yoshida, *Eur. J. Org. Chem.* **2008**, 2564–2570; l) J. Luo, T. Lei, L. Wang, Y. Ma, Y. Cao, J. Wang, J. Pei, *J. Am. Chem. Soc.* **2009**, *131*, 2076–2077; m) N. Shiota, T. Kinuta, T. Sato, N. Tajima, R. Kuroda, Y. Matsubara, Y. Imai, *Cryst. Growth Des.* **2010**, *10*, 1341–1345.
- [3] T. Kinuta, K. Kamon, T. Harada, Y. Nakano, N. Tajima, T. Sato, M. Fujiki, R. Kuroda, Y. Matsubara, Y. Imai, *Eur. J. Org. Chem.* **2009**, 5760–5764.
- [4] a) B. Valeur, *Molecular Fluorescence*, Wiley-VCH, Weinheim, **2005**; b) H. Langhals, T. Potrawa, H. Nöth, G. Linti, *Angew. Chem.* **1989**, *101*, 497–499; *Angew. Chem. Int. Ed. Engl.* **1989**, *28*, 478–480; c) H. Langhals, R. Ismael, O. Yürük, *Tetrahedron* **2000**, *56*, 5435–5441; d) K. Yoshida, Y. Ooyama, H. Miyazaki, S. Watanabe, *J. Chem. Soc. Perkin Trans. 2* **2002**, 700–707; e) H.-C. Yeh, W.-C. Wu, Y.-S. Wen, D.-C. Dai, J.-K. Wang, C.-T. Chen, *J. Org. Chem.* **2004**, *69*, 6455–6462; f) Y. Ooyama, T. Okamoto, T. Yamaguchi, T. Suzuki, A. Hayashi, K. Yoshida, *Chem. Eur. J.* **2006**, *12*, 7827–7838; g) Y. Ooyama, K. Yoshida, *Eur. J. Org. Chem.* **2008**, 2564–2570.
- [5] Determined by PLATON geometry calculation.
- [6] C. Rafel, N. Carmen, *Chem. Rev.* **2007**, *107*, 874–922.
- [7] A. D. Becke, *J. Chem. Phys.* **1993**, *98*, 5648–5652.
- [8] a) T. H. Dunning, Jr., *J. Chem. Phys.* **1989**, *90*, 1007–1023; b) D. E. Woon, T. H. Dunning Jr., *J. Chem. Phys.* **1993**, *98*, 1358–1371.
- [9] a) J. E. Ridley, M. C. Zerner, *Theor. Chim. Acta* **1973**, *32*, 111–134; b) J. E. Ridley, M. C. Zerner, *Theor. Chim. Acta* **1976**, *42*, 223–236; c) M. C. Zerner, G. H. Lowe, R. F. Kirchner, U. T. Mueller-Westerhoff, *J. Am. Chem. Soc.* **1980**, *102*, 589–599.
- [10] Gaussian 03, Revision E.01, M. J. Frisch, G. W. Trucks, H. B. Schlegel, G. E. Scuseria, M. A. Robb, J. R. Cheeseman, J. A. Montgomery, Jr., T. Vreven, K. N. Kudin, J. C. Burant, J. M. Millam, S. S. Iyengar, J. Tomasi, V. Barone, B. Mennucci, M. Cossi, G. Scalmani, N. Rega, G. A. Petersson, H. Nakatsuji, M. Hada, M. Ehara, K. Toyota, R. Fukuda, J. Hasegawa, M. Ishida, T. Nakajima, Y. Honda, O. Kitao, H. Nakai, M. Klene, X. Li, J. E. Knox, H. P. Hratchian, J. B. Cross, V. Bakken, C. Adamo, J. Jaramillo, R. Gomperts, R. E. Stratmann, O. Yazyev, A. J. Austin, R. Cammi, C. Pomelli, J. W. Ochterski, P. Y. Ayala, K. Morokuma, G. A. Voth, P. Salvador, J. J. Dannenberg, V. G. Zakrzewski, S. Dapprich, A. D. Daniels, M. C. Strain, O. Farkas, D. K. Malick, A. D. Rabuck, K. Raghavachari, J. B. Foresman, J. V. Ortiz, Q. Cui, A. G. Baboul, S. Clifford, J. Cioslowski, B. B. Stefanov, G. Liu, A. Liashenko, P. Piskorz, I. Komaromi, R. L. Martin, D. J. Fox, T. Keith, M. A. Al-Laham, C. Y. Peng, A. Nanayakkara, M. Challacombe, P. M. W. Gill, B. Johnson, W. Chen, M. W. Wong, C. Gonzalez, J. A. Pople, Gaussian, Inc., Wallingford CT, **2004**.
- [11] R. Kuroda, Y. Saito, *Bull. Chem. Soc. Jpn.* **1976**, *49*, 433–436.
- [12] G. M. Sheldrick, SHELXL97, *Acta Crystallogr. Sect. A* **2008**, *64*, 112–122.
- [13] A. L. Spek, *PLATON*, A Multipurpose Crystallographic Tool, Utrecht University, Utrecht, Netherlands; **2010**.
- [14] G. M. Sheldrick, *SADABS*, Program for Empirical Absorption Correction of Area Detector Data, University of Göttingen, Germany, **1996**.

Received: October 26, 2010

Published online: January 24, 2011